coatings

MDPI

Article

Friction and Wear Behavior of an Ag–Mo Co-Implanted GH4169 Alloy via Ion-Beam-Assisted Bombardment

Jiajun Zhu *, Meng Xu, Wulin Yang, Deyi Li, Lingping Zhou and Licai Fu *

College of Materials Science and Engineering, Hunan University, Changsha 410082, China; xumeng@hnu.edu.cn (M.X.); hnuywl@hnu.edu.cn (W.Y.); lideyi@hnu.edu.cn (D.L.); lpzhou@hnu.edu.cn (L.Z.)
* Correspondence: tft@hnu.edu.cn (J.Z.); lfu@hnu.edu.cn (L.F.); Tel./Fax: +86-731-8882-2663 (J.Z. & L.F.)

Academic Editors: Braham Prakash and Jens Hardell
Received: 12 September 2017; Accepted: 2 November 2017; Published: 6 November 2017

Abstract: Ag, Mo, and Ag–Mo were respectively implanted into GH4169 alloy substrates without heating via ion-beam-assisted bombardment technology (IBAB). In addition, the wear performance under low sliding speed and applied load were researched at room temperature (RT). A small amount silver molybdate phase could be detected on the surface of the co-implanted GH4169 alloy bombarded by a high-energy ion beam. The average friction coefficients under the steady wear state had almost no change at all. Compared with the un-implanted GH4169 alloys, the wear rate of the GH4169 alloys with co-implantation of Ag and Mo was reduced by 75%. A large amount of the silver molybdate phase could be generated due to the tribo-reaction on the worn surface during sliding. It benefits the formation of continuous oxide layers as lubrication and protected layers, leading to the change in the predominant wear mechanism from abrasion and adhesion wear to oxidation wear.

Keywords: GH4169 alloy; Ag–Mo co-implantation; ion-beam-assisted bombardment technology (IBAB); wear mechanism

1. Introduction

In order to achieve a low-friction coefficient and wear rate for some harsh-condition applications, numerous works on the lubrication effects about the addition of solid lubricant phases to metal matrices, such as graphite, oxides, soft metals, MoS_2, and fluoride, have been carried out [1–7]. Double metal oxides, including titanates, tungstates, molybdate, and vanadates, are effective high-temperature solid lubricants [8–11]. Among these double metal oxides, more attention has been paid to silver molybdate, which possesses a layer-like structure, because of its excellent lubrication performance, achieving low friction at high temperatures [2,9–17]. For example, Liu et al. [11] investigated the tribological properties of Ni-based self-lubricating composites containing Ag and MoS_2 within a wide temperature range. The evolution of the friction coefficient from room temperature (RT) to 700 °C ranges from 0.18 to 0.77, and the coefficient decreases down to 0.18 at 700 °C as temperature increases. The wear rate from RT to 700 °C is reduced by an order of magnitude, and the worn surface is covered by a continuous and smooth film at 700 °C. As temperature increases to 500 °C, MoS_2 is oxidized and becomes molybdenum oxide. Ag and Mo oxide generates silver molybdate, first proposed by Gulbinski [18], good high-temperature lubrication with a layered structure, which may be considered a mixture of AgO and MoO_3 layers separated by a silver layer. In fact, the lubrication mechanism of silver molybdate can be attributed to weaker Ag–O bridging bonds that are more easily broken to form a rich silver lubrication film when subjected to sliding, which is responsible for the low friction at the sliding interface [9]. Ni-based composites with an addition of lubricious Ag_2MoO_4 at various temperatures have also been explored. Due to high-temperature fabrication processing, Ag_2MoO_4 decomposes but is reproduced in the rubbing process at high temperatures, leading to an improvement in tribological performance. Thus, at 700 °C, the lowest friction coefficient can be

observed (about 0.26). Furthermore, Chen [2] and Aouadi [13] studied adaptive NiCrAlY–Ag–Mo coatings and nanocomposite $Mo_2N/MoS_2/Ag$ coatings, respectively. Friction coefficients for both coatings can be lowered to 0.1 at 600 °C due to the formation of silver molybdate on the worn surface during sliding. Due to the large enthalpy of formation (ΔH_f = +57 kJ/mol), silver molybdate usually forms during sliding at high temperatures and works as an effective high-temperature solid lubricant.

In this study, ion-beam-assisted bombardment (IBAB), an unbalanced process, makes it possible to produce intermetallic compounds or intermediate phases at RT [19–21]. In fact, a silver molybdate phase formed via the co-implanted GH4169 alloy during the preparation process in our experiments, but only a small amount was produced, which may be related to the high surface atomic activity of the Ag and Mo particles on the surface. In addition, a series of tribo-reactions promoted the production of more silver phase on the worn surface during the sliding process. Usually, the powder metallurgy process as a high-temperature fabrication method leads to the decomposition of silver molybdate [11]. The generation of silver molybdate at RT during preparation and sliding has considerable significance, but such generation has scarcely been reported. Moreover, the RT lubrication performance of silver molybdate in the form of a film has not been investigated as much.

This work focuses on the tribological properties of a GH4169 alloy co-implanted with Ag and Mo prepared via IBAB at RT. For comparison, a single Ag and a single Mo are implanted into the same alloy, respectively. A correlation analysis and a discussion of the tribo-chemical reaction on the worn surface and effects on the wear behavior are given. The wear mechanism is further revealed as well.

2. Experimental Details

2.1. Sample Preparation

The chemical compositions of the commercial GH4169 alloy, provided by Beijing Iron and Steel Research Institute, are shown in the following Table 1.

Table 1. The chemical compositions of the GH4169 alloy.

Chemical Element	Weight Percentage (wt %)
Fe	20.2
Cr	16.8
Nb	4.95
Mo	2.81
Ti	0.78
Al	0.46
Si	0.49
Ni	balance

The polished 15 mm × 15 mm × 5 mm GH4169 alloy substrates were implanted with Ag, Mo, and Ag–Mo via IBAB. These preparation experiments were performed on a homemade multi-functional ion beam system (MIS800, Sykeyou Vacuum Technology Institute, Shenyang, China), the structure schematic of which is shown in Figure 1. Two Kaufman ion sources (named sputtering ion sources 1 and 2) were respectively used for sputtering an Ag target (purity > 99.99%) and an Mo target (purity > 99.9%) with a 2.5 keV Ar^+ ion beam. A third Kaufman ion source (named the assisted ion source) was used for bombarding the particles into the alloy surface via an Ar^+ ion beam with an accelerating voltage of about several tens of thousands of volts, which was incident along the normal direction of the base surface. The purity of argon as a working gas was about 99.999%, and the working pressures during deposition with single and double targets was set to 1.5×10^{-2} Pa and 2.3×10^{-2} Pa, respectively. The experimental time was 1 h. The implanted samples were numbered in accordance with the implanted particle, as shown in Table 2. The un-implanted alloy was marked as N.

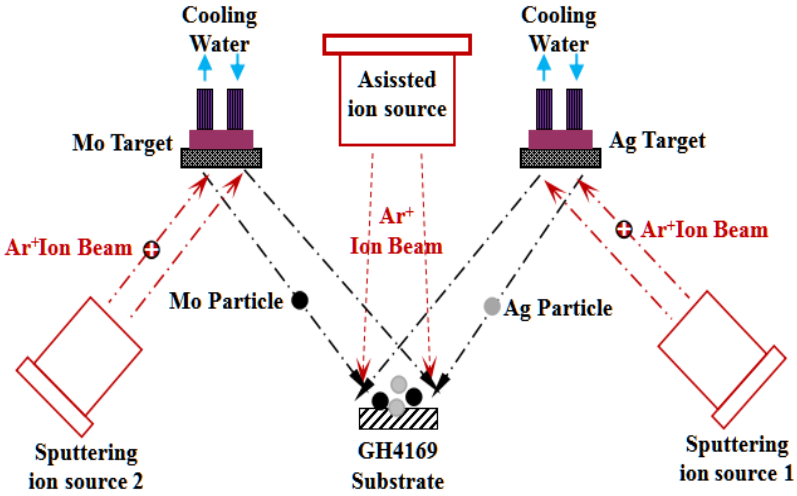

Figure 1. Schematic diagram of the multi-functional ion beam deposition system.

Table 2. The particles implanted into GH4169 alloy substrates and the numbering.

Sample	Particle Implanted into the GH4169 Alloy
A	Silver
M	Molybdenum
AM	Silver and molybdenum

2.2. Friction and Wear Test

The friction coefficients of all samples were measured under a normal load of 2 N in atmospheric conditions at RT with a wear tribometer (WTM-2E, Lanzhou Institute of Chemical Physics, Lanzhou, China) in a ball-on-disk style (a relative humidity of 70% ± 5%). The wear test was conducted in a circular motion 5 mm in diameter under a fixed sliding speed of 47 mm/s. The upper ball was a counterpart Si_3N_4 ball 5 mm in diameter with a hardness of 19 GPa. Hertzian contact pressure was 1.2 GPa, according to our calculations. The single wear test time was 10 min and was repeated five times. The friction coefficient curves were recorded automatically with a computer attached to the tribometer. After the wear test, the Wyko NT9100 surface profiler (Chung Ming Automation Equipment Co., Ltd., Shanghai, China) was used to obtain the profiles of the wear tracks. The wear rate was calculated as the equation $\omega = \Delta V/(F \cdot L)$, ω was the wear rate in $mm^3 \cdot N^{-1} \cdot m^{-1}$, ΔV was the wear volume loss in mm^3, L was the total motion distance in m, and F was the load in N.

2.3. Characterization

The structures and the phase compositions of all samples were analyzed with an X-ray diffractometer (XRD, D500, Bruker, Beijing, China) with a 40 kV operating voltage and Cu Kα radiation in the 2θ range of 25°–80°. The chemical states before the friction test were examined with an X-ray photoelectron spectroscope (XPS, PHI-5702, Thermo Fisher Scientific, Waltham, MA, USA). The Raman spectrometer (Labram-010, an excitation wavelength of 632 nm, HORIBA, Beijing, China) further surveyed the phase constitutions of all samples before and after the wear test. The elemental compositions of selected regions and the morphologies of the wear tracks for all samples were analyzed using a scanning electron microscope (SEM, JSM-6700F, JEOL, Beijing, China), equipped with backscattered electrons (BSEs) and an energy dispersive spectrometer (EDS).

3. Result and Discussion

3.1. Composition and Microstructure

The XRD patterns of all samples before the wear test are presented in Figure 2, which includes the un-implanted GH4169 alloy. It was found that the γ matrix phase could be observed in all samples, which mainly came from the GH4169 alloy. In Figure 2ab, the characteristic peaks of Ag (2θ = 37.92°) and Mo (2θ = 40.56°) correspond to FCC Ag (111) and BCC Mo (110), respectively, excluding the GH4169 base. Both Ag (111) and Mo (110) peaks have a smaller angle shift. It may be related to the lattice distortion induced by the bombardment of the high-energy ion beam. Moreover, the XRD results of the co-implanted GH4169 alloy allowed us to identify the Ag and Mo phases in the co-implanted sample (Figure 2d).

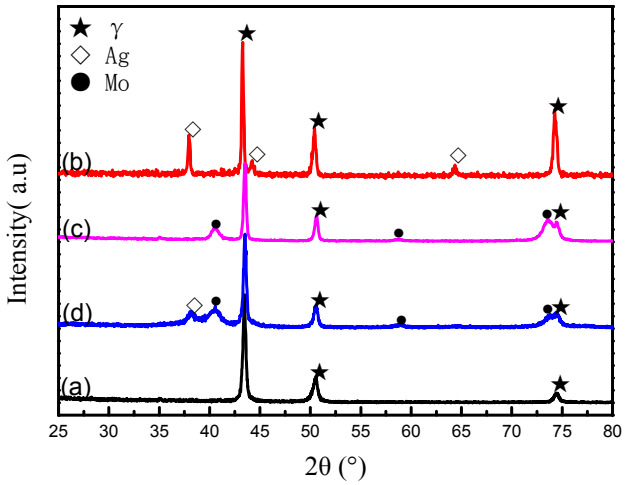

Figure 2. XRD spectra of (**a**) the un-implanted alloy (N); (**b**) silver (A); (**c**) molybdenum (M); and (**d**) silver and molybdenum (AM) before the wear test.

Figure 3a, in which peaks derived from O, Ag, and Mo are all evident, exhibits the XPS full spectrum for the co-implanted GH4169 alloy before the wear test. As can be seen in Figure 3b, the XPS peaks of Ols at 531.8 eV and 530.5 eV yielded two Ag_2MoO_4 Gaussian peaks. The $Ag3d_{5/2}$ and $3d_{3/2}$ peaks deviate from those of the Ag-implanted sample (Figure 3c), indicating that the binding energy of $Ag3d_{5/2}$ and $3d_{3/2}$ slightly shifted to a lower value. Similarly, the $Mo3d_{5/2}$ and $3d_{3/2}$ peaks deviate from those of the Mo-implanted sample (Figure 3d). Based on the Ag3d peak position, the peaks at 368.18 eV and 374.23 eV can be assigned to $Ag3d_{5/2}$ and $3d_{3/2}$ in the Ag_2MoO_4 phase, respectively. In addition, the peaks located at 232.73 eV and 235.93 eV can be assigned to $Mo3d_{5/2}$ and $3d_{3/2}$ in Ag_2MoO_4, respectively. This result is consistent with reports of Suthanthiraraj and Liu [11,22].

Compared with the XPS result above, no obvious characteristic peaks of the Ag_2MoO_4 phase were found in the XRD pattern of AM before sliding. This may be due to the low content and good dispersion of Ag_2MoO_4. To confirm this, the phase compositions of AM were determined via a laser Raman spectrometer (Figure 4). Monoclinic silver molybdate with a broad peak can be detected with Raman spectra [2,11–13]. We inferred that silver molybdate indeed formed during the preparation process. Because of the bombardment of the high-energy ion beam, the co-deposited particles on the base surface have substantially high activity. The chemical reaction between Ag, Mo, and the residual oxygen from the vacuum chamber or the oxygen adsorbed on the base surface might happen under an unbalanced fabrication process at RT. XPS and Raman analysis reveal that silver molybdate can be generated directly via ion-beam-assisted bombardment at RT.

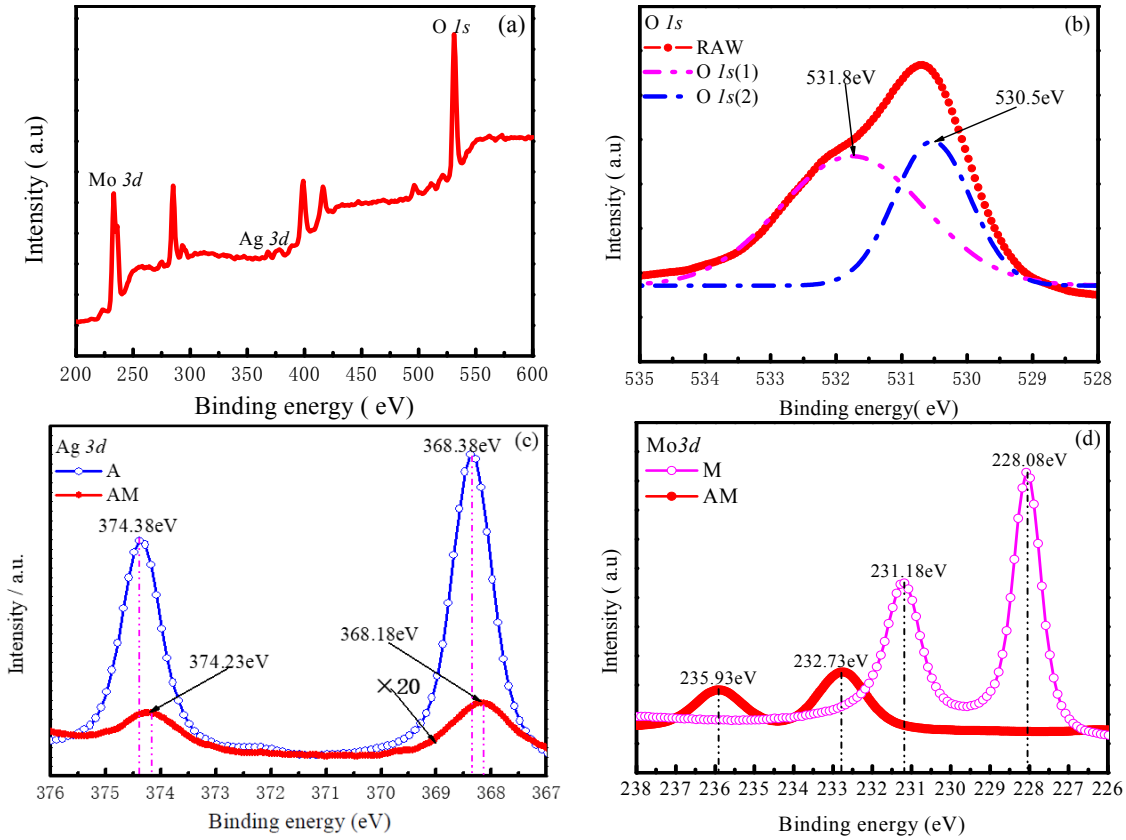

Figure 3. (**a**) XPS full spectra; (**b**) O1s XPS spectra for AM; (**c**) Ag3d XPS spectra of A and AM; and (**d**) Mo3d XPS spectra of M and AM before the wear test.

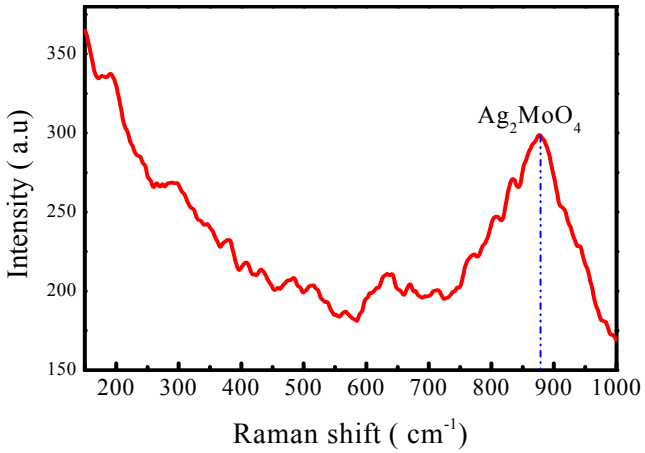

Figure 4. Raman spectra of AM before the wear test.

3.2. Friction and Wear Properties

Figure 5a presents the friction coefficient evolution of all samples with sliding time under a normal load of 2 N. Compared with the bare GH4169 alloy (N), the AM shows a lower friction coefficient at the beginning of the test, which is attributed to the formation of silver molybdate with an atomically layered structure during the wear test. As the test proceeded, the friction coefficient steadily increased to reach the base nature. The average friction coefficient and wear rate under the dry friction and RT conditions are presented in Figure 5b for all samples. Compared with the bare GH4169 alloy, there is no obvious change in the average friction coefficient at the steady wear state. It was speculated that the

Ag-implanted sample has a smaller mean friction coefficient due to the synergistic lubrication effect of Ag and Ag_2O. The wear rate of the co-implanted sample (AM) was the lowest of all samples, as shown in Figure 5b, from 4.88 × 10^{-4} $mm^3 \cdot N^{-1} \cdot m^{-1}$ to 1.22 × 10^{-4} $mm^3 \cdot N^{-1} \cdot m^{-1}$ compared with the base, due to the presence of silver molybdate. The wear rate for the Mo-implanted sample is much higher, the highest of all the samples, than that of the base. It is also estimated that MoO_3 formed on the worn surface leads into the worst anti-wear performance for M. Research shows that MoO_3 is brittle and has no lubrication at low temperature [23].

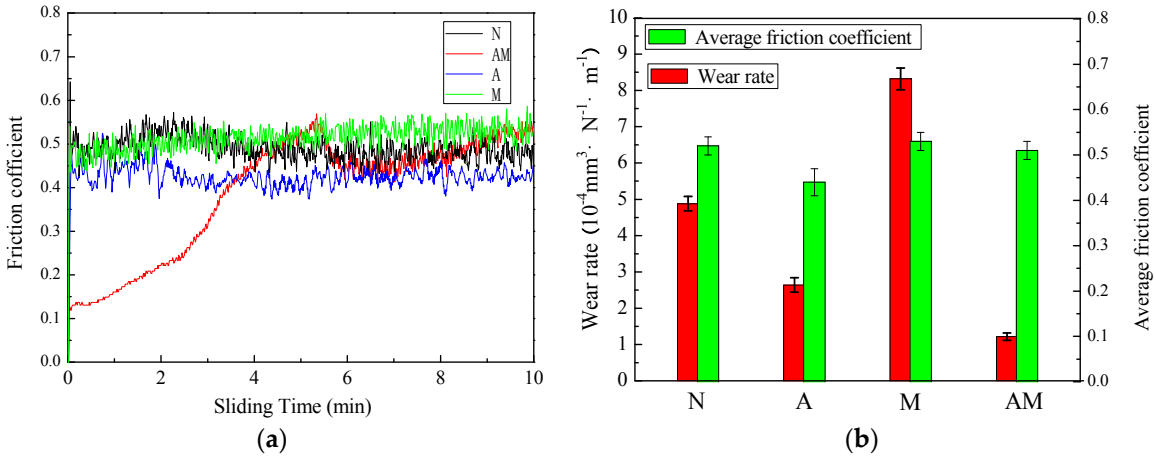

Figure 5. (**a**) The friction coefficient and (**b**) the average friction coefficient and wear rate for all samples tested under a normal load of 2 N and a fixed sliding speed of 47 mm/s.

Figure 6 displays the cross-section profiles and surface 3D topographies of the wear scars for all samples after the 10 min friction test. Among all samples, the sample AM exhibits the smoothest wear tracks with the smallest wear volumes as seen in Figure 6d, indicating the best wear resistance performance. The visible adhesive marks are observed on the selected zone marked with a red box for the worn surface of N, A, and M as seen from Figure 6a–c. The Mo-implanted sample shows the deepest wear tracks (Figure 6c), which is consistent with Figure 5.

The SEM morphologies of the wear tracks after sliding are given for all samples in Figure 7. The selected dark zone (named I) and gray zone (named II) on the wear scars for all samples were analyzed with EDS. The oxygen element was enriched in the dark regions. In Figure 7a, the worn surface is characterized with small bumps and delamination pits, indicating abrasive wear and brittle fracture in the bare GH4169 alloy. The discontinuous dark regions covering the surface in Figure 7b are believed to be the discontinuous oxide layer. It can be inferred that the predominant wear mechanism for A is oxidation and adhesive wear. The Mo-implanted sample, accompanied by a large amount of the wear debris and some abrasive grooves on the worn surface, exhibits the most serious wear condition (Figure 7c). The continuous tribo-layer covered on the worn surface, together with some shallow grooves for the co-implanted sample, can be seen in Figure 7d. As discussed before, the continuous oxide layers (the corresponding continuous dark regions) formed in AM with the smoothest wear scar, which accounts for the lower wear rate. The formation of a tribo-layer, as a protective and lubricating layer [24], can effectively reduce the direct contact of the sample and the Si_3N_4 ball. It has been illustrated that the oxidation wear dominates the wear processing of the co-implanted GH4169 alloy [25].

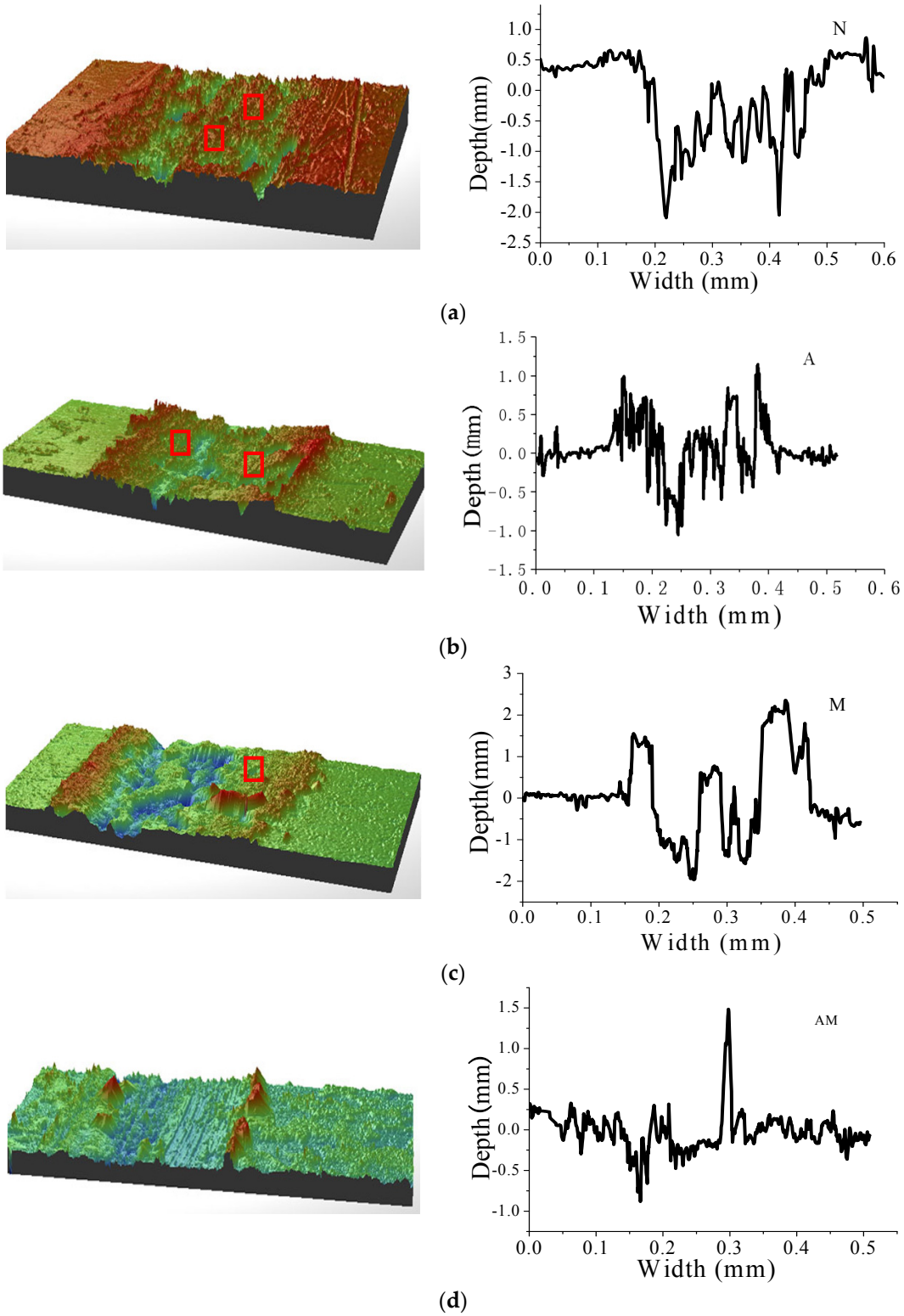

Figure 6. The cross-section profiles, surface 3D topographies of wear tracks for (**a**) N, (**b**) A, (**c**) M, and (**d**) AM after the wear test.

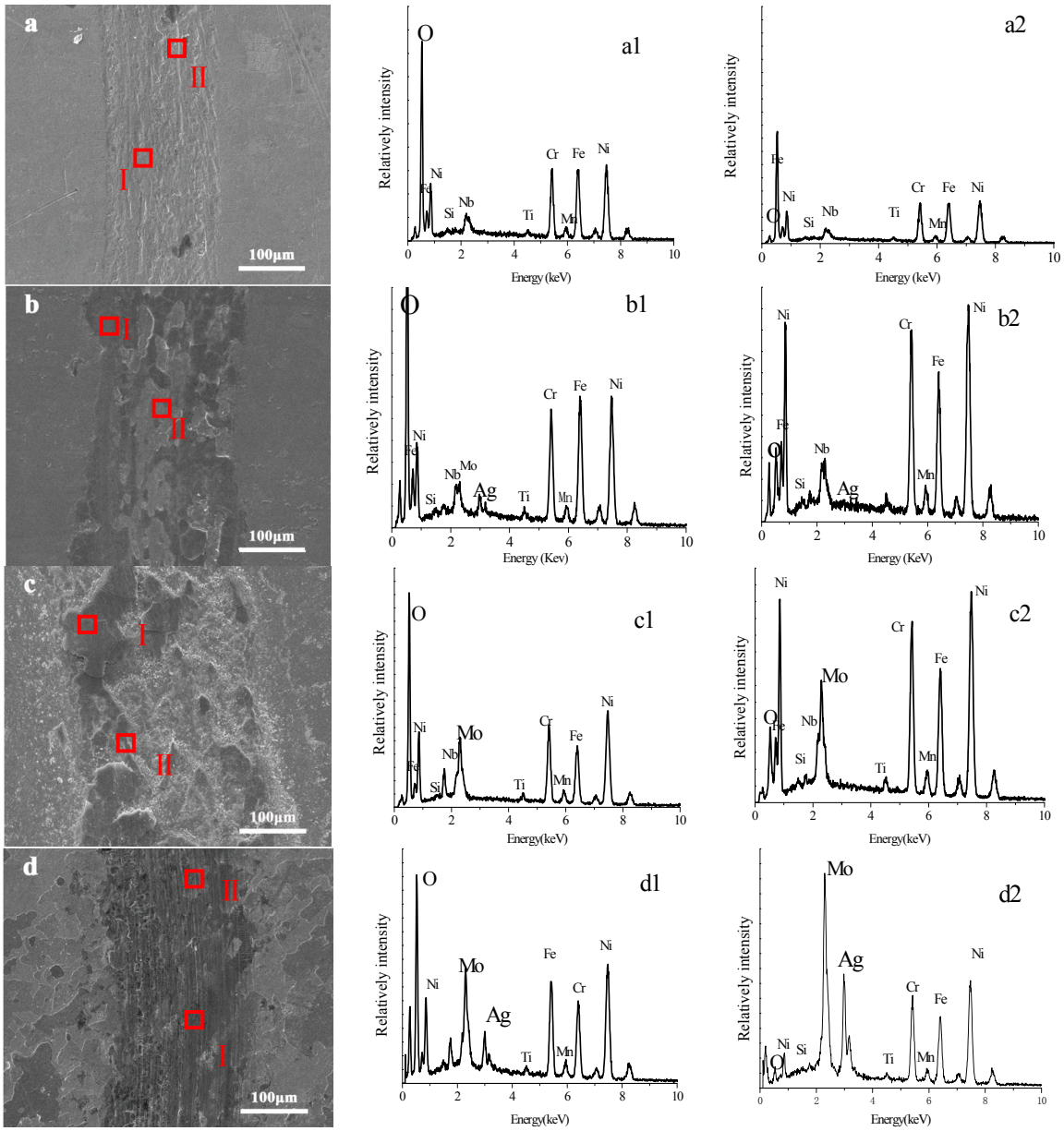

Figure 7. The SEM micrographs of the worn surfaces after the fiction test for (**a**) N, (**b**) A, (**c**) M, and (**d**) AM.

Adhesion wear can be seen in the SEM images in Figure 8 on the worn surface of the counterface ball against the AM. The SEM image of the worn surface of the counterface ball against A presents clear abrasion wear. This is because, as the wear test continued, the contact between the counterface and the sample (A and AM) led to material transfer via adhesive wear. Table 3 shows the chemical compositions of the counterface balls determined via EDS, providing further evidence for oxidation wear and material transfer via adhesion wear.

The tribo-chemical reactions and phase changes on the worn surfaces were further studied with the micro-Raman. In the following Raman spectra (Figure 9a), Fe_2O_3, resulting from the oxidation of Fe and Cr in the matrix, can be detected on the worn surfaces of all samples. The generation of Fe_2O_3 is expected to contribute to the lubricating effect [23,26,27]. Ag_2O and MoO_3 can be found on the worn surfaces, respectively, of A and M. In addition, the Ag_2MoO_4 phase is detected on the worn surface after the sliding process of AM. It has been inferred that silver molybdate can be combined via

tribo-reaction between MoO_3 and Ag on high-energy-contacted surfaces during RT wear tests [2,11]. Based on the Raman spectra of the sample surfaces, as shown in Figure 9b, before and after the wear test, the peak intensity of Ag_2MoO_4 increased substantially after the friction test of AM. It can be inferred that Ag_2MoO_4 content rose after the wear test due to the further generation of Ag_2MoO_4 during sliding. That the Ag_2MoO_4 phase can be synthesized during the preparation and rubbing processes is also demonstrated.

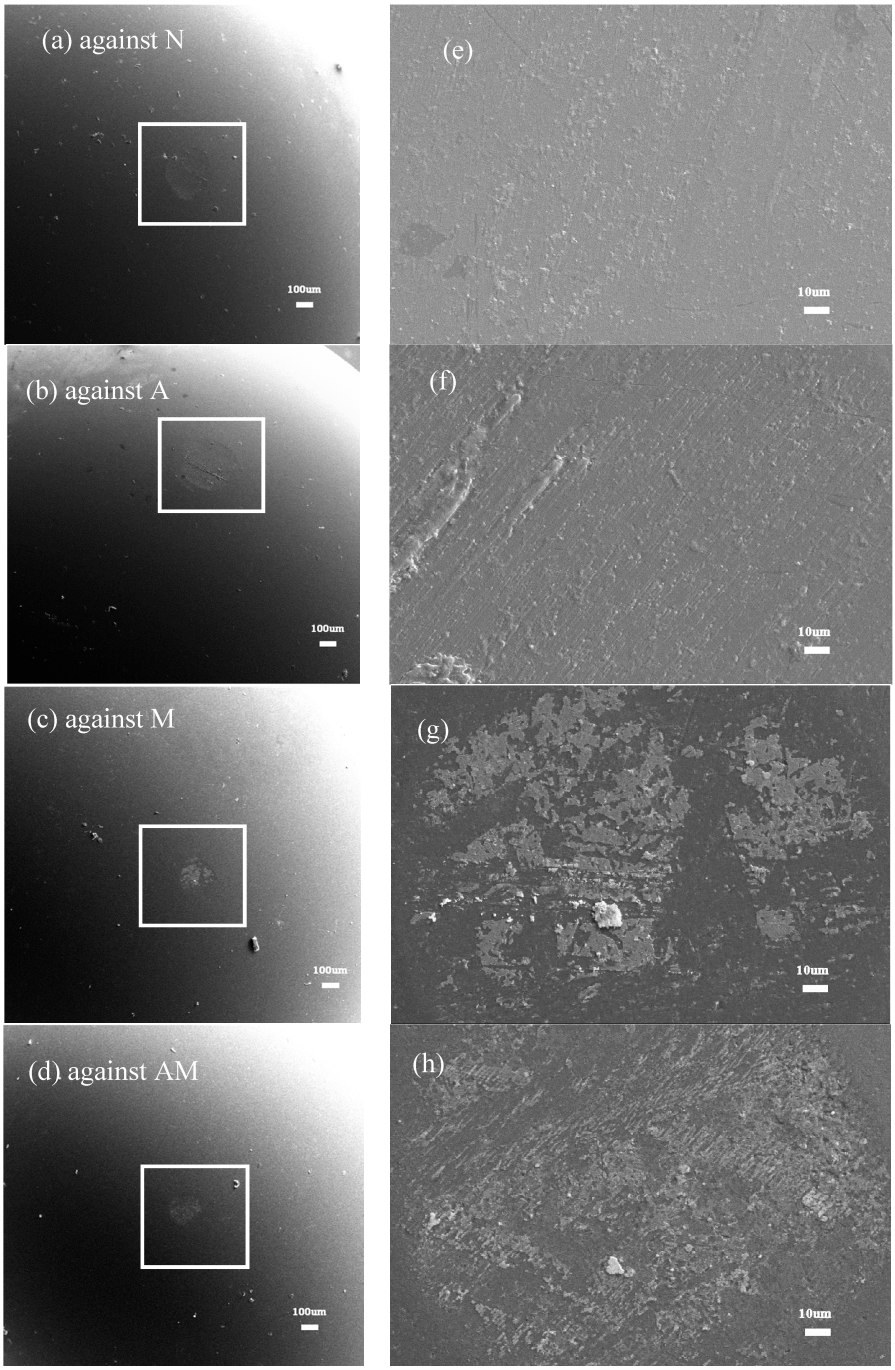

Figure 8. The SEM images of the counterface balls (Si_3N_4 ball) after sliding against (**a**) A, (**b**) B, (**c**) C, and (**d**) D and corresponding higher magnification SEM images against (**e**) A, (**f**) B, (**g**) C, and (**h**) D.

Table 3. The element compositions of the worn surfaces of all counterface balls.

Sample	Element Composition (at.%)							
	Si	N	Ni	Fe	O	Ag	Al	Mo
N	72.96	7.36	0.61	0.17	16.62	0	2.27	0
A	56.54	19.78	0.89	1.27	19.19	0.43	1.91	0
M	74.41	6.21	0.55	0.66	16.29	0	1.87	0
AM	56.14	14.8	0.33	0.55	23.28	0.99	1.98	1.93

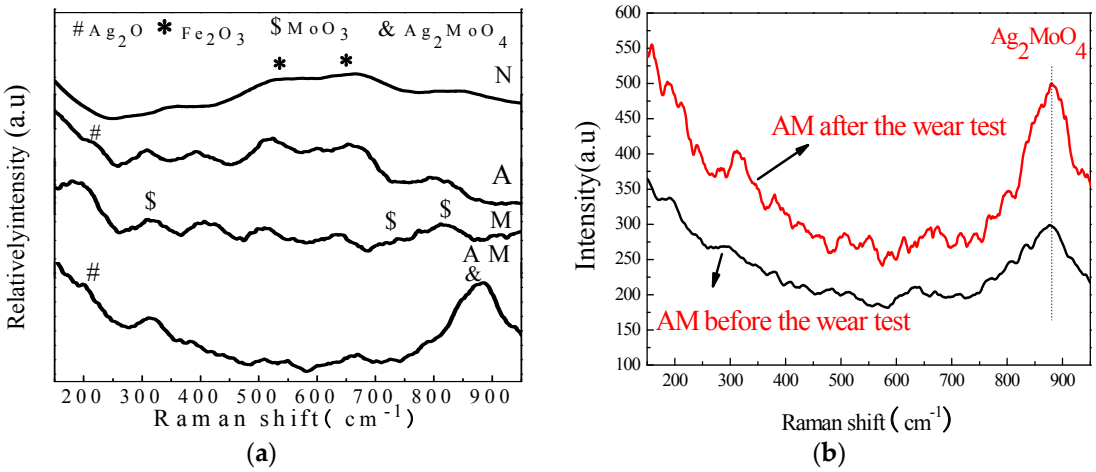

Figure 9. (**a**) Raman spectra of the worn surfaces for all samples after the wear test; and (**b**) Raman spectra before and after the wear test for AM.

As demonstrated above, the unbalanced fabrication method results in the generation of Ag_2MoO_4 during the preparation process at RT. In addition, more silver molybdate formed on the worn surface of AM during the RT friction-wear test through a series of tribo-chemical reactions on the high-energy-contacted surface. The co-implanted sample has the best wear resistance performance, attributed to the formation of Ag_2MoO_4. In the friction test, the wear mechanism was dominant by oxidation wear in AM covered by a continuous oxide layer. A large amount of silver molybdate with a layered structure [11,28], formed on the worn surface during sliding, promotes the formation of a continuous oxide film. Furthermore, the Ag_2MoO_4 phase with weaker Ag–O bridging bonds can easily break to form rich silver lubrication layers at a lower wear rate. It is generally known that silver molybdate is an excellent high-temperature solid lubricant, and little research on the lubrication behavior of Ag_2MoO_4 at RT has been conducted. However, our experimental results prove that silver molybdate can greatly improve the wear resistance performance at RT.

4. Conclusions

By ion-beam-assisted bombardment technology, the GH4169 alloy implanted with Ag, Mo, and Ag–Mo, respectively, were prepared at RT. The microstructure, phase compositions, tribological behavior and mechanism were investigated. The conclusions drawn are as follows:

- Compared with GH4169 alloy substrates, the wear resistance of the GH4169 alloy co-implanted with Ag and Mo was effectively enhanced, which is attributed to the production of Ag_2MoO_4 with a layer-like structure, easily forming a rich silver lubrication layer during sliding.
- The predominant wear mechanism changed from abrasion and adhesion wear to oxidation wear due to the silver lubrication layer and continuous oxide layers found on the worn surface of the co-implanted GH4169 alloy.

- During the preparation process and sliding at RT, the formation of silver molybdate can be achieved through ion-beam-assisted bombardment, an unbalanced preparation method.

Acknowledgments: The authors acknowledge the financial support from the National Natural Science Foundation of China (51401080 and 51675169).

Author Contributions: Jiajun Zhu and Licai Fu conceived and designed the experiments; Lingping Zhou performed the experiments; Jiajun Zhu and Licai Fu analyzed the data; Wulin Yang and Deyi Li contributed reagents/materials/analysis tools; Jiajun Zhu and Meng Xu wrote the paper.

Conflicts of Interest: The authors declare no conflict of interest.

References

1. An, Y.; Chen, J.; Hou, G.; Zhao, X.; Zhou, H.; Chen, J.; Yan, F. Effect of silver content on tribological property and thermal stability of HVOF-sprayed nickel-based solid lubrication coating. *Tribol. Lett.* **2015**, *58*, 34. [CrossRef]
2. Chen, J.; An, Y.; Yang, J.; Zhao, X.; Zhou, H.; Chen, J.; Yan, F. Tribological properties of adaptive NiCrAlY–Ag–Mo coatings prepared by atmospheric plasma spraying. *Surf. Coat. Technol.* **2013**, *235*, 521–528. [CrossRef]
3. Yin, H.; Xu, Y.; Li, X.; Chang, W.; Zhou, Y. Design of friction and wear resistant titanium- and cobalt-modified nickel-base repair alloys by spray forming. *Mater. Des.* **2017**, *116*, 403–410. [CrossRef]
4. Scharf, T.W.; Prasad, S.V. Solid lubricants: A review. *J. Mater. Sci.* **2013**, *48*, 511–531. [CrossRef]
5. Cheng, J.; Zhen, J.; Zhu, S.; Yang, J.; Ma, J.; Li, W.; Liu, W. Friction and wear behavior of Ni-based solid-lubricating composites at high temperature in a vacuum environment. *Mater. Des.* **2017**, *122*, 405–413. [CrossRef]
6. Zhu, S.; Li, F.; Ma, J.; Cheng, J.; Yin, B.; Yang, J. Tribological properties of Ni_3Al matrix composites with addition of silver and barium salt. *Tribol. Int.* **2015**, *84*, 118–123. [CrossRef]
7. Zhu, S.; Bi, Q.; Yang, J.; Liu, W. Effect of fluoride content on friction and wear performance of Ni_3Al matrix high-temperature self-lubricating composites. *Tribol. Lett.* **2011**, *43*, 341–349. [CrossRef]
8. Stone, D.S.; Harbin, S.; Mohseni, H.; Mogonye, J.E.; Scharf, T.W.; Muratore, C. Lubricious silver tantalate films for extreme temperature applications. *Surf. Coat. Technol.* **2013**, *217*, 140–146. [CrossRef]
9. Gao, H.Y.; Otero-De-La-Roza, A.; Gu, J.J.; Stone, D.A.; Aouadi, S.M. (Ag,Cu)–Ta–O ternaries as high-temperature solid-lubricant coatings. *ACS Appl. Mater. Interfaces* **2015**, *7*, 15422–15429. [CrossRef] [PubMed]
10. Liu, E.-Y.; Wang, W.-Z.; Gao, Y.-M.; Jia, J.-H. Tribological properties of adaptive Ni-based composites with addition of lubricious Ag_2MoO_4 at elevated temperatures. *Tribol. Lett.* **2012**, *47*, 21–30. [CrossRef]
11. Liu, E.-Y.; Wang, W.-Z.; Gao, Y.-M.; Jia, J.-H. Tribological properties of Ni-based self-lubricating composites with addition of silver and molybdenum disulfide. *Tribol. Int.* **2013**, *57*, 235–241. [CrossRef]
12. Bondarev, A.V.; Kiryukhantsev-Korneev, P.V.; Sidorenko, D.A.; Shtansky, D.V. A new insight into hard low friction MoCN–Ag coatings intended for applications in wide temperature range. *Mater. Des.* **2016**, *93*, 63–72. [CrossRef]
13. Aouadi, S.M.; Paudel, Y.; Simonson, W.J.; Ge, Q.; Kohli, P.; Muratore, C. Tribological investigation of adaptive $Mo_2N/MoS_2/Ag$ coatings with high sulfur content. *Surf. Coat. Technol.* **2009**, *203*, 1304–1309. [CrossRef]
14. Chen, F.; Feng, Y.; Shao, H.; Zhang, X.; Chen, J.; Chen, N. Friction and Wear Behaviors of $Ag/MoS_2/G$ Composite in Different Atmospheres and at Different Temperatures. *Tribol. Lett.* **2012**, *47*, 139–148. [CrossRef]
15. Gulbiński, W.; Suszko, T. Thin films of MoO_3–Ag_2O binary oxides—The high temperature lubricants. *Wear* **2006**, *261*, 867–873. [CrossRef]
16. Jie, C.; Zhao, X.; Zhou, H. HVOF-sprayed adaptive low friction NiMoAl–Ag coating for tribological application from 20 to 800 °C. *Tribol. Lett.* **2014**, *56*, 55–66.
17. Li, B.; Gao, Y.; Han, M.; Guo, H.; Wang, W.; Jia, J. Microstructure and tribological properties of NiCrAlY-Mo-Ag composite by vacuum hot-press sintering. *Vacuum* **2017**, *143*, 1–6. [CrossRef]
18. Gulbinski, W.; Suszko, T.; Sienicki, W.; Warcholinski, B. Tribological properties of silver- and copper-doped transition metal oxide coatings. *Wear* **2003**, *254*, 129–135. [CrossRef]

19. Figueroa, R.; Abreu, C.M.; Cristóbal, M.J.; Pena, A. Effect of nitrogen and molybdenum ion implantation in the tribological behavior of AA7075 aluminum alloy. *Wear* **2012**, *276*, 53–60. [CrossRef]
20. Onate, J.I.; Alonso, F.; Garcia, A. Improvement of tribological properties by ion implantation. *Thin Solid Films* **1998**, *317*, 471–476. [CrossRef]
21. Zhao, B.; Li, D.M.; Zeng, F.; Pan, F. Ion beam induced formation of metastable alloy phases in Cu–Mo system during ion beam assisted deposition. *Appl. Surf. Sci.* **2003**, *207*, 334–340. [CrossRef]
22. Suthanthiraraj, S.A.; Premchand, Y.D. Molecular structural analysis of 55mol% CuI-45mol% Ag_2MoO_4, solid electrolyte using XPS and laser Raman techniques. *Ionics* **2004**, *10*, 254–257. [CrossRef]
23. Muratore, C.; Voevodin, A.A.; Hu, J. Tribology of adaptive nanocomposite yttria-stabilized zirconia coatings containing silver and molybdenum from 25 to 700 °C. *Wear* **2006**, *261*, 797–805. [CrossRef]
24. Zhang, Q.-Y.; Zhou, Y.; Wang, L.; Cui, X.-H.; Wang, S.-Q. Investigation on tribo-layers and their function of a titanium alloy during dry sliding. *Tribol. Int.* **2016**, *94*, 541–549. [CrossRef]
25. Kato, H. Effects of supply of fine oxide particles onto rubbing steel surfaces on severe-mild wear transition and oxide film formation. *Tribol. Int.* **2008**, *41*, 735–742. [CrossRef]
26. Gupta, S.; Filimonov, D.; Zaitsev, V.; Palanisamy, T.; El-Raghy, T.; Barsoum, M.W. Study of tribofilms formed during dry sliding of Ta_2AlC/Ag or Cr_2AlC/Ag composites against Ni-based superalloys and Al_2O_3. *Wear* **2009**, *267*, 1490–1500. [CrossRef]
27. Hardell, J.; Hernandez, S.; Mozgovoy, S.; Pelcastre, L.; Courbon, C.; Prakash, B. Effect of oxide layers and near surface transformations on friction and wear during tool steel and boron steel interaction at high temperatures. *Wear* **2015**, *330–331*, 223–229. [CrossRef]
28. Stone, D.; Liu, J.; Singh, D.P.; Muratore, C.; Voevodin, A.A.; Mishra, S. Layered atomic structures of double oxides for low shear strength at high temperatures. *Scr. Mater.* **2010**, *62*, 735–738. [CrossRef]